Journal of Clinical and Translational Hepatology **2021** vol. 9(3) | 315–323
DOI: 10.14218/JCTH.2020.00173

Original Article

Differentiation of Hepatocellular Carcinoma from Hepatic Hemangioma and Focal Nodular Hyperplasia using Computed Tomographic Spectral Imaging

Weixia Li[1#], Ruokun Li[1#], Xiangtian Zhao[2#], Xiaozhu Lin[3], Yixing Yu[4], Jing Zhang[1], Kemin Chen[1], Weimin Chai[1] and Fuhua Yan[1*]

[1]Department of Radiology, Ruijin Hospital Affiliated to Shanghai Jiao Tong University School of Medicine, Shanghai, China; [2]Department of Radiology, Guangdong General Hospital, Guangdong Academy of Medical Sciences, Guangzhou, Guangdong, China; [3]Department of Nuclear Medicine, Ruijin Hospital affiliated to Shanghai Jiao Tong University School of Medicine, Shanghai, China; [4]Department of Radiology, The First Affiliated Hospital of Soochow University, Suzhou, Jiangsu, China

Received: 21 December 2020 | **Revised:** 26 February 2021 | **Accepted:** 7 March 2021 | **Published:** 31 March 2021

Abstract

Background and Aims: Hepatocellular carcinoma (HCC) is the most common primary hepatic malignancy. This study was designed to investigate the value of computed tomography (CT) spectral imaging in differentiating HCC from hepatic hemangioma (HH) and focal nodular hyperplasia (FNH). ***Methods:*** This was a retrospective study of 51 patients who underwent spectral multiple-phase CT at 40–140 keV during the arterial phase (AP) and portal venous phase (PP). Slopes of the spectral curves, iodine density, water density derived from iodine- and water-based material decomposition images, iodine uptake ratio (IUR), normalized iodine concentration, and the ratio of iodine concentration in liver lesions between AP and PP were measured or calculated. ***Results:*** As energy level decreased, the CT values of HCC (*n*=31), HH (*n*=17), and FNH (*n*=7) increased in both AP and PP. There were significant differences in IUR in the AP, IUR in the PP, normalized iodine concentration in the AP, slope in the AP, and slope in the PP among HCC, HH, and FNH. The CT values in AP, IUR in the AP and PP, normalized iodine concentration in the AP, slope in the AP and PP had high sensitivity and specificity in differentiating HH and HCC from FNH. Quantitative CT spectral data had higher sensitivity and specificity than conventional qualitative CT image analysis during the combined phases. ***Conclusions:*** Mean CT values at low energy (40–90 keV) and quantitative analysis of CT spectral data (IUR in the AP) could be helpful in the differentiation of HCC, HH, and FNH.

Citation of this article: Li W, Li R, Zhao X, Lin X, Yu Y, Zhang J, *et al*. Differentiation of hepatocellular carcinoma from hepatic hemangioma and focal nodular hyperplasia using computed tomographic spectral imaging. J Clin Transl Hepatol 2021;9(3):315–323. doi: 10.14218/JCTH.2020.00173.

Introduction

Hepatocellular carcinoma (HCC) is the most common primary hepatic malignant tumor and the third leading cause of cancer-related death worldwide, with annual mortality rates of 14.3 per 100,000 men and 5.1 per 100,000 women.[1,2] Hepatic hemangioma (HH) and focal nodular hyperplasia (FNH) are the most and the second most common benign hepatic lesions.[3–5] Since the three lesions may share some characteristics upon imaging examination, the differentiation of HCC from HH and FNH is very critical, as their clinical courses, prognosis, and treatment are markedly different.

About 80–90% of HCCs occur as a complication of chronic liver disease, secondary to viral hepatitis B- or C-induced cirrhosis or alcoholic cirrhosis; therefore, patient clinical history may be helpful for the differential diagnosis of HCC from HH and FNH.[6–8] Nevertheless, the remaining 10–20% of HCCs can be found in a low-risk population or in patients without alcohol abuse. Besides, typical HCC, HH, and FNH can be diagnosed with confidence using ultrasound, contrast-enhanced computed tomography (CT), or magnetic resonance imaging (commonly known as MRI),[9–21] but in some instances, HCC may display atypical imaging presentations if the tumor is well-differentiated,[22,23] small (≤2 cm),[24] with fatty metamorphosis,[25,26] or with abundant interstitial fibrosis.[10,27,28] In addition, HH may show slow enhancement or homogeneous enhancement during the arterial phase (AP),[29–32] while atypical FNH may show non-enhancement of the central scar, less intense enhancement of the tumor, and pseudo-capsular enhancement in delayed images.[33] In the presence of atypical imaging appearances, it may not be easy to distinguish HCC from HH and FNH.

Keywords: Hepatocellular carcinoma; Hepatic hemangioma; Focal nodular hyperplasia; Computed tomography spectral imaging; Spectral curve.

Abbreviations: AP, arterial phase; AUC, the area under the ROC curve; CNR, contrast-to-noise ratio; CT, computed tomography; DECT, dual-energy computed tomography; FNH, focal nodular hyperplasia; GSI, gemstone spectral imaging; HCC, hepatocellular carcinoma; HH, hepatic hemangioma; ICR, iodine concentration ratio; ID, iodine density; IUR, iodine uptake ratio; LNR, lesion-to-normal parenchyma ratio; MD, material decomposition; MRI, magnetic resonance imaging; NIC, normalized iodine concentrations; PACS, picture archiving and communication system; PP, portal venous phase; ROC, receiver operating characteristic; ROI, Regions of interest; WD, water density.

[#]These authors contributed equally to this work.

[*]**Correspondence to:** Fuhua Yan, Department of Radiology, Ruijin Hospital Affiliated to Shanghai Jiao Tong University School of Medicine, 197 Ruijin Erlu, Huangpu District, Shanghai 200025, China. ORCID: https://orcid.org/0000-0002-6385-499X. Tel: +86-21-6437-0045-665724, Fax: +86-21-6384-2916, E-mail: yfh11655@rjh.com.cn

Many studies have shown superior performance of MRI over conventional CT in the diagnosis of HCC;[34,35] however, it may be contraindicated in some patients or may result in insufficient image quality in some patients with ascites or patients incapable of holding their breath. With the introduction of dual-energy CT (commonly referred to as DECT) spectral imaging in the field of liver imaging, several studies have shown the benefit of DECT in the improved evaluation of microvascular invasion in HCC,[36] in the visualization and quantification of HCC,[37] and in the early detection of HCC and hypervascular liver tumors[38–40] DECT improved soft tissue contrast by generating different monochromatic images,[41,42] which also showed that material decomposed images could provide increased contrast in the visualization of the AP hyperenhancement and washout in HCC compared to both monoenergetic 65 keV images and MRI.[37] Until now, only a few studies have reported spectral CT being used in differentiating small HH,[43,44] FNH[45] or angiomyolipoma[46] from HCC with only a few parameters, such as the contrast-to-noise ratio, normalized iodine concentrations (referred to as NIC), and lesion-to-normal parenchyma iodine concentration ratio. Nevertheless, there is almost no literature about systematic and comprehensive comparisons using CT attenuation values derived from a set of monochromatic images (40–140 keV) and other quantitative assessments, including iodine density (referred to as ID), water density (referred to as WD), and the slopes of the spectral curve between HCC, HH, and FNH.

Therefore, this study aimed to describe CT attenuation values derived from a set of monochromatic images and material density-related quantitative assessments for HCC, HH, and FNH, and to evaluate the value of CT spectral imaging in distinguishing HCC from HH and FNH.

Methods

Patients

This retrospective study included patients with known or suspected liver tumors, who underwent dynamic enhancement CT scanning in gemstone spectral imaging (GSI) mode on a Discovery CT750 HD scanner (GE Healthcare, Chicago, IL, USA) between February 2012 and January 2018. The exclusion criteria were: 1) no HCC, HH, or FNH; 2) no histological confirmation; 3) with prior trans-arterial chemoembolization or radiofrequency ablation; or 4) recurrent HCC after liver resection or transplantation. This study was approved by the ethics committee of Ruijin Hospital Affiliated to Shanghai Jiao Tong University School of Medicine. Individual consent was waived because of the retrospective nature of the study.

Diagnostic procedures

All HCCs were confirmed pathologically after surgical resection. The HCCs were graded according to the Edmondson-Steiner classification.[47] The diagnosis of HH was established based on histological specimens obtained at partial hepatectomy or typical multiple-phase CT findings, including peripheral nodular enhancement similar to the enhancement of blood vessels at the AP and centripetal fill-in enhancement at the portal venous phase (PP). FNH was proven pathologically after surgical resection because of diagnostic uncertainty after MRI or initial misdiagnosis as HCC.

CT examinations

All patients underwent triple-phase CT within a maximum of 10 days of surgery, using the high-definition Discovery CT750 HD scanner. The detailed scan parameters are provided in the online supplementary materials. Three types of images were reconstructed from the single spectral CT acquisition for analysis, namely conventional polychromatic images obtained at 140 kVp, iodine- and water-based material decomposition (referred to as MD) images, and a set of monochromatic images obtained with energy levels ranging from 40 to 140 keV.

Quantitative analyses

All measurements were performed on an advanced workstation (AW 4.4; GE Healthcare) using the GSI viewer software, by a single radiologist experienced in abdominal radiology and blind to the results of all patients. The 70 keV monochromatic images and iodine-based MD images were reviewed first. Regions of interest (referred to as ROIs) were placed in the lesions, normal liver parenchyma, and aorta on the default 70-keV monochromatic images (Fig. 1). The GSI viewer software automatically calculated the mean CT attenuation value and standard deviation at different energy levels (40–140 keV, at 10-keV intervals) from the set of monochromatic image and ID and WD values from the iodine- and water-based (IDM and WDM, respectively) images during AP and PP.[48] Four parameters were obtained from the measurements of CT values and iodine concentration. The NIC during AP was calculated as ratio of the iodine concentrations in AP in the lesions and aorta. Iodine concentrations in the lesions in AP were normalized to those of the aorta in order to minimize variations among patients. The iodine uptake ratio (IUR) was calculated as the ratio of the mean iodine concentrations in the lesions and in the non-tumor hepatic parenchyma surrounding the lesion. The iodine concentration ratio (ICR) in liver lesions between AP and PP was calculated as the difference of the iodine concentrations in the lesions during AP and PP. The slopes of the spectral curve in AP and PP were calculated as $(CT_{40keV}-CT_{90keV})/50$, where CT_{40keV} and CT_{90keV} were the mean CT attenuation values in the lesions at 40 keV and 90 keV of the spectral curves, respectively.

Qualitative analysis

Two radiologists (WXL and XTZ, with 15 and 14 years of experience in abdominal CT imaging, respectively) qualitatively reviewed the 70 keV monochromatic images by consensus with the GSI viewer at the workstation. Neither observer was aware of clinical, surgical, and pathologic findings. The observers documented the following enhancement and morphologic features: number; maximal diameter on transverse images; necrosis or cyst; scar; and, enhancement pattern and degree. The enhancement patterns and degrees were evaluated for any enhancing portion of the lesion relative to the aorta and the adjacent liver parenchyma during AP and relative to the adjacent liver parenchyma during PP. The enhancement patterns were described as globular or nodular, diffuse homogeneous, or heterogeneous. The enhancement degree of the lesion was classified as hyper-, iso-, or hypo-enhancement compared with surrounding liver parenchyma. The changes in enhancement degree between AP and PP were characterized as expansion, washout, or none. The expansion was defined as a hyperenhancement area in the lesion during both AP and PP. Washout was defined as a change from hyper- or iso-enhancement area in the lesion during AP to a hypo-enhancement area in the lesion compared with surrounding liver parenchyma during PP, while none was defined as a hyper- or iso-enhancement

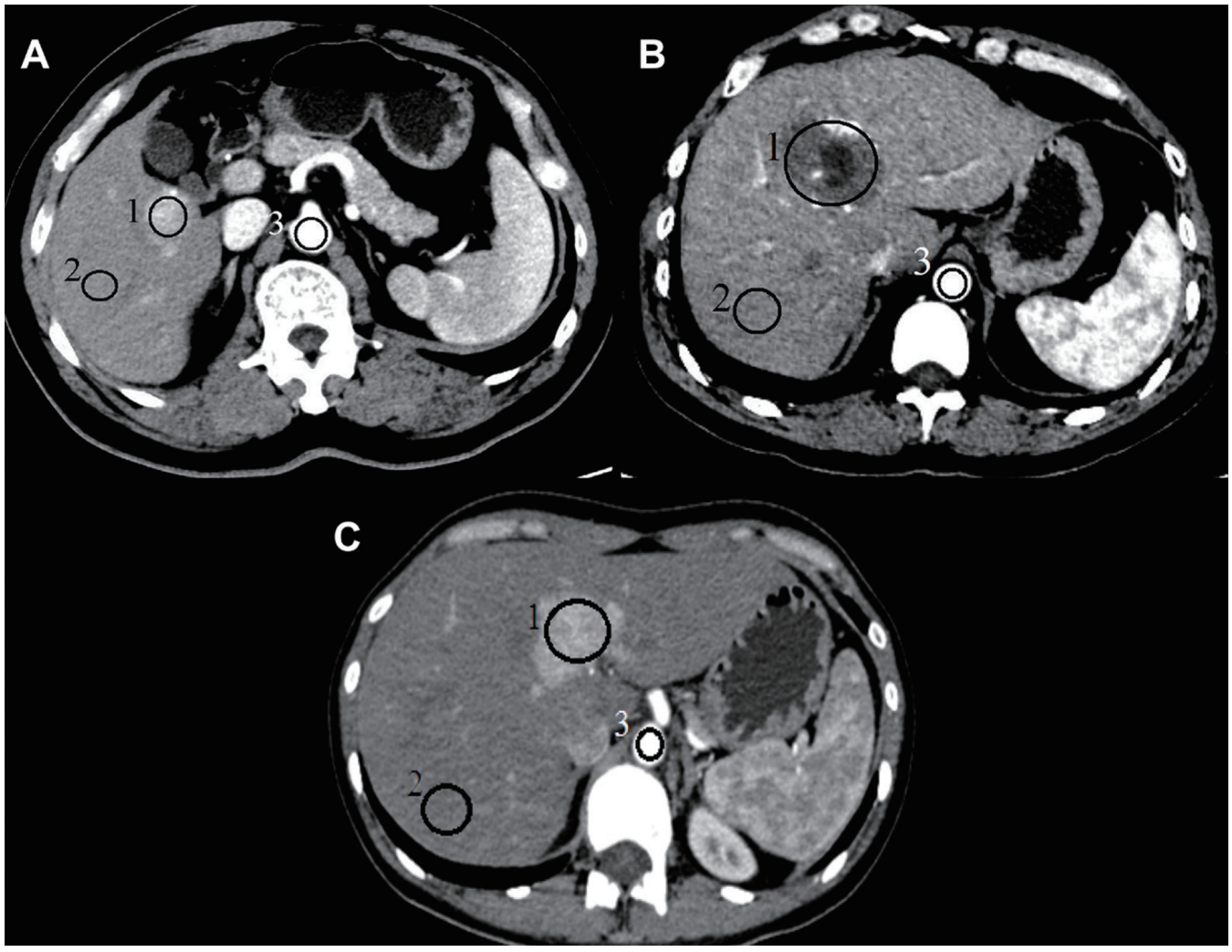

Fig. 1. DECT imaging of liver lesions. Circular or elliptical ROIs were placed in the lesion (#1), normal hepatic parenchyma (#2), and aorta (#3) on the default 70-keV monochromatic images. DECT, dual-energy computed tomography; ROI, region of interest.

area in the lesion during AP to an iso-enhancement area in the lesion compared with adjacent liver parenchyma during PP.

Finally, the observers, in consensus, characterized each lesion type as HCC, HH, and FNH based on imaging features (online supplementary materials). Differences among the observers were resolved by means of consensus discussion. The definition of the sensitivity and specificity for differential diagnosis of HCC, HH and FNH are demonstrated in the online supplementary materials.

Statistical analysis

The data were analyzed using SPSS 13.0 (SPSS Inc., Chicago, IL, USA). Continuous variables were presented as median (interquartile range) after confirming their non-normal distribution using the Kolmogorov-Smirnov test. The estimated parameters were analyzed among HCC, HH, and FNH groups using the Kruskal-Wallis test, with the Wilcoxon rank-sum post hoc test. Receiver operating characteristic (ROC) curves were used to help establish the threshold values of the mean CT values at different energy levels (40–140 keV), IDM, WDM, IUR and slope in AP, and PP, and ICR required for significant differentiation of HCC, HH, and FNH. The diagnostic capability was determined by calculating the area under the ROC curve (AUC). The best sensitivity and specificity were determined using the optimal thresholds based on the Youden's index. A two-sided p value of <0.05 was considered statistically significant. Qualitative CT imaging features were compared among HCC, HH, and FNH by Fisher's exact tests.

Results

Patients

From 476 potentially eligible patients, 425 were excluded based on the following exclusion criteria: 1) no HCC, HH, or FNH; 2) no histological confirmation; 3) with prior transarterial chemoembolization or radiofrequency ablation; or 4) recurrent HCC after liver resection or transplantation. Therefore, 51 patients (30 males and 21 females) were included, with 31 HCCs in 31 patients, 17 HHs in 13 patients, and 7

Table 1. Characteristics of the patients

Variable	HCC, *n*=31	HH, *n*=13	FNH, *n*=7
Number of lesions	31	17	7
Age in years, median (IQR)	57.0 (16.0)	48.0 (18.0)	24.0 (11.0)
Male, *n* (%)	26 (83.4)	2 (15.4)	2 (28.6)
Background liver status, *n* (%)			
Normal liver	2 (6.5)	13 (100)	7 (100)
Cirrhosis	29 (93.5)	0	0
Cause, *n* (%)			
HBV infection	28 (90.3)	0	0
HBV and alcoholic cirrhosis	1 (9.7)	0	0
Tumor size in cm, median (IQR)	3.00 (3.00)	5.30 (3.35)	5.00 (2.00)

FNH, focal nodular hyperplasia; HBV, hepatitis B virus; HCC, hepatocellular carcinoma; HH, hepatic hemangioma; IQR, interquartile range.

FNHs in 7 patients (Table 1). According to the Edmondson-Steiner classification, two HCCs were grade I, fourteen were grade II, thirteen were grade III, and two were grade IV. All patients who were diagnosed as HH with multiple-phase CT findings were followed for at least 3 years. No patient was lost to follow-up.

Quantitative analysis

CT values: Regarding the CT values of HCC, HH, and FNH, there was a trend towards a decrease in mean CT values of HH, HCC, and FNH as energy level increased (40–140 keV) in both AP and PP (Table 2 and Fig. 2). HH had the lowest mean CT values, while FNH had the highest mean CT values at different energy levels (40–140 keV) in both AP and PP (Table 2 and Fig. 2). Moreover, there were significant differences in CT values at energy levels from 40 to 140 keV during AP and PP (Table 2) for HCC vs. FNH, and HH vs. FNH. There were significant differences between HCC and HH at energy levels from 40 to 140 keV in AP and only at energy levels from 40 to 100 keV in PP (Table 2).

ROC curve analysis revealed that the mean CT values from 40–140 keV in both AP and PP, especially at 40–120 keV in AP (all AUC=1) and 120 keV in PP (AUC=0.992) had the best performance in differentiating HH from FNH. The mean CT values at 80–90 keV in AP (both AUC=0.926) and 100 keV in PP (AUC=0.949) had better performance in differentiating HCC from FNH. Meanwhile, the mean CT values at 40–50 keV in AP (AUC=0.896) and 40–50 keV in PP (AUC=0.780) had high sensitivity and specificity in differentiating HCC from HH. See Supplementary Tables S1–S3.

Standard deviation of the mean CT values: For the standard deviation of the mean CT values of HCC, HH, and FNH in AP and PP (Table 3), there were significant differences at 40 to 100 keV during PP between HCC and HH, and from 40 to 140 keV during PP between HH and FNH. In addition, sensitivity (88.2%) and specificity (100%) showed that the standard deviation of mean CT values at 40 keV in PP (AUC=0.882) had the best performance in differentiating HH from FNH. The standard deviation of mean CT values from 40–140 keV in PP showed low sensitivity and specificity in differentiating between HCC and FNH. The standard deviation of mean CT values at 40–100 keV in PP, especially at 50 keV (AUC=0.846), had the best sensitivity and specificity in differentiating between HCC and HH. See Supplementary Tables S4–S6.

Quantitative assessments

For the spectral CT imaging-specific quantitative assessments of HCC, HH, and FNH, there were significant differences in IUR, slope in AP and PP, NIC in AP (which tended to increase from HH, HCC to FNH) between every two groups of HCC, HH, and FNH (Table 4). IDM in both AP and PP, WDM in PP, and ICR revealed significant differences between HH and FNH, as well as IDM in AP and PP, and ICR between HH and HCC, WDM in PP between HCC and FNH also differed significantly (Table 4). ROC curve analysis demonstrated that ICR and slope in AP had the best diagnostic performance (AUC=0.992) in differentiating HH from FNH. While IUR in AP had better performance (AUC=0.903) in differentiating HCC from FNH. For distinguishing HCC from HH, IDM and slope in AP, ICR had good performance (AUC=0.890). See Supplementary Tables S7–S9.

Qualitative analysis

The CT features of the HH, HCC, and FNH groups were analyzed and listed in Table 5. Feeding vessels were found in 15 (48.4%) of the 31 HCCs, 6 (85.7%) of the 7 FNHs, and none was found in HHs (both $p<0.001$ for HCC vs. HH, FNH vs. HH, respectively). Thirteen (76.5%) of seventeen HHs showed globular or nodular enhancement during AP, whereas neither HCCs nor FNHs showed it (both $p<0.001$ for HH vs. HCC and for HH vs. FNH). Fourteen (82.4%) of seventeen HHs demonstrated expansion change of enhancement between AP and PP ($p<0.001$ for HH vs. HCC and $p=0.001$ HCC vs. FNH, respectively), whereas twenty-two (71%) of the thirty-one lesions of HCC demonstrated washout change of enhancement between AP and PP ($p<0.001$ for HH vs. HCC and $p=0.001$ for HCC vs. FNH, respectively).

In the conventional qualitative analysis of imaging features with combined AP and PP, we achieved sensitivity of 83.9% (26 of 31 HCCs) and specificity of 82.4% (14 of 17 HHs), respectively, for differentiating between HCC and HH, which was lower than quantitative image analysis with CT spectral imaging, which had sensitivity of 87.1% and specificity of 88.2%. Meanwhile, for differentiating between FNH and HH, we achieved sensitivity of 76.5% (13 of 17 HHs) vs. 100%, specificity 71.4% (5 of 7 FNHs) vs. 100%. In addition, we achieved sensitivity of 80.6% (25 of 31 HCCs) vs. 100%, and specificity 71.4% (5 of 7 FNHs) vs. 90.3%, respectively.

Table 2. Mean CT attenuation values of HCC, HH, and FNH at energy levels ranging 40–140 keV (at 10-keV intervals) during AP and PP

Energy in keV	HH, *n*=17	HCC, *n*=31	FNH, *n*=7	*p*		
				HCC vs. HH	HCC vs. FNH	FNH vs. HH
AP						
40	102.77 (57.02)	210.02 (125.86)	318.74 (165.34)	<0.001*	0.004*	<0.001*
50	81.67 (36.37)	156.48 (83.43)	224.71 (113.64)	<0.001*	0.003*	<0.001*
60	66.45 (23.41)	115.87 (57.17)	166.84 (71.39)	<0.001*	0.006*	<0.001*
70	59.31 (17.24)	95.09 (41.81)	130.42 (42.74)	<0.001*	0.001*	<0.001*
80	54.65 (15.29)	81.35 (29.19)	113.65 (26.49)	<0.001*	<0.001*	<0.001*
90	48.65 (15.52)	71.15 (23.73)	103.64 (16.13)	<0.001*	<0.001*	<0.001*
100	47.45 (16.05)	65.59 (22.63)	90.07 (15.13)	<0.001*	0.001*	<0.001*
110	46.99 (15.41)	61.76 (20.84)	78.06 (17.20)	0.002*	0.001*	<0.001*
120	45.56 (15.06)	58.96 (20.06)	69.62 (18.75)	0.004*	0.001*	<0.001*
130	44.08 (14.76)	56.62 (17.53)	65.52 (21.27)	0.008*	0.002*	<0.001*
140	42.89 (14.21)	53.91 (16.29)	62.56 (23.54)	0.018*	0.004*	<0.001*
PP						
40	179.57 (89.33)	246.44 (78.64)	338.48 (63.72)	0.001*	0.004*	0.001*
50	131.95 (58.34)	176.12 (50.17)	238.85 (38.62)	0.001*	0.002*	0.001*
60	102.98 (40.96)	132.85 (36.90)	177.56 (32.60)	0.002*	0.001*	0.001*
70	84.44 (28.58)	105.22 (25.08)	142.38 (28.65)	0.003*	0.001*	0.001*
80	72.55 (22.82)	87.80 (19.26)	114.83 (26.14)	0.004*	<0.001*	<0.001*
90	64.49 (19.53)	74.59 (16.54)	98.60 (24.60)	0.010*	<0.001*	<0.001*
100	59.04 (18.46)	66.74 (16.56)	87.38 (23.48)	0.036*	<0.001*	<0.001*
110	54.73 (17.71)	60.70 (16.34)	79.44 (22.23)	0.065	<0.001*	<0.001*
120	50.80 (16.64)	56.48 (15.14)	73.88 (21.25)	0.113	0.001*	<0.001*
130	47.87 (15.76)	53.57 (13.83)	69.62 (21.17)	0.185	0.001*	<0.001*
140	47.05 (15.01)	50.92 (13.13)	66.25 (21.36)	0.200	0.002*	0.001*

Data are expressed as median (interquartile range). *p<0.05. AP: arterial phase; FNH, focal nodular hyperplasia; HCC, hepatocellular carcinoma; HH, hepatic hemangioma.

Discussion

The present study suggests that spectral CT can be helpful for differentiating HCC from HH and FNH. HH had the lowest mean CT values, while FNH had the highest mean CT values at different energy levels. The different slopes clearly indicated that the CT spectral imaging could distinguish HCC, HH, and FNH.

Treatment options and the prognosis of HCC, HH, and FNH are markedly different. Previous studies discussed the role of CT in the diagnosis of HCC, HH, and FNH,[9,11,19,20,30–33] but they were primarily focusing on analyzing the imaging features of the lesions qualitatively. Some studies reported quantitative evaluations of spectral CT in differentiating small HH,[43] FNH,[45] or angiomyolipoma[46] from HCC with only a few parameters. This study systematically and comprehensively compared CT values derived from a set of monochromatic images (from 40 to 140 keV at 10-keV intervals), and quantitative assessments including ID, WD, and the slopes of the spectral curve for differentiating HCC, HH, and FNH. The study expands the results of previous studies[43,45,46] that only examined spectral CT features of HCC vs. one lesion type and with limited energy levels. This is supported by Wang *et al*.,[48] who showed that spectral CT features could differ between malignant and benign liver lesions.

The present study shows that the mean CT values and the standard deviation of mean CT values measured on monochromatic images at low energy levels (40–90 keV), especially in AP, have better contrast resolution compared to monochromatic images at high energy levels (100–140 keV). This means that the CT values and their standard deviation (which represent the heterogeneity of lesions in CT values) measured on monochromatic images at certain energy levels could be helpful for the differential diagnosis of different hypervascular hepatic tumors. This is partly similar to the studies reported by Lv *et al*.[40] and Yu *et al*.,[45] who found that monochromatic images at energy levels of 40–70 keV could improve the differential diagnosis of small HCC compared to conventional polychromatic images. ROC curve analysis in the study also confirmed that quantitative analysis of CT spectral data had higher sensitivity and specificity with those of conventional qualitative CT image analysis during combined phases for differentiating HCC, FNH and HH.

According to the present study results, all values of IUR in the AP for HCC, FNH, and HH were >1, which means that all three groups showed hyperenhancement appearance during AP. The value of IUR in the PP of HCC was <1 during

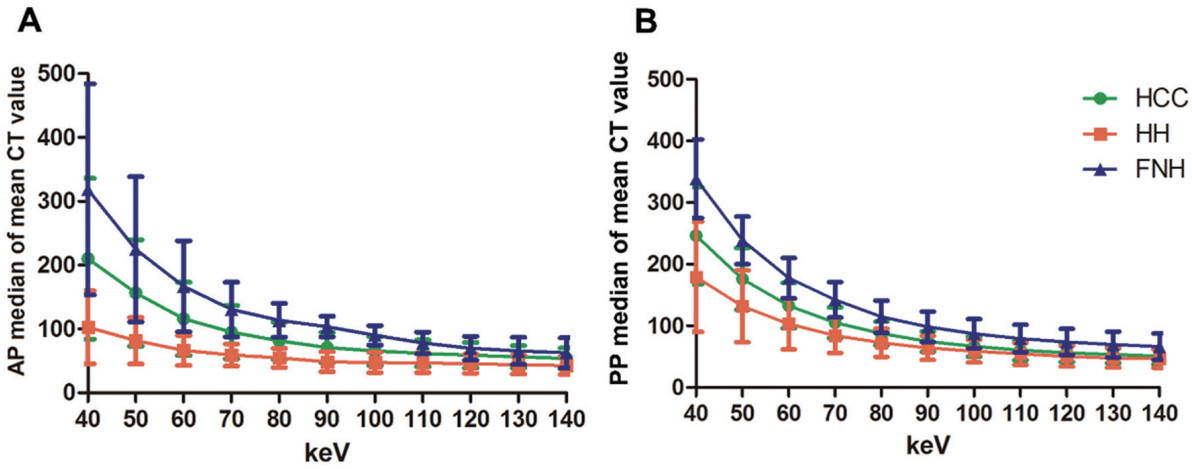

Fig. 2. Spectral curves of HH, HCC, and FNH in AP and PP. (A) The spectral curves of HH, HCC, FNH at different energy levels (40–140 keV). CT values peaked at 40 keV and decreased as photon energy increased in the AP for all three lesions. (B) The spectral curves of HH, HCC, and FNH at different energy levels (40–140 keV). CT values peaked at 40 keV and decreased as photon energy increased in the PP for all three lesions. AP, arterial phase; FNH, focal nodular hyperplasia; HCC, hepatocellular carcinoma; HH, hepatic hemangioma; PP, portal venous phase.

Table 3. Standard deviations of mean CT attenuation values (the heterogeneity of lesions in mean CT values) of HCC, HH, and FNH at energy levels ranging 40–140 keV (at 10-keV intervals) during AP and PP

Energy in keV	HH, *n*=17	HCC, *n*=31	FNH, *n*=7	*p*		
				HCC vs. HH	HCC vs. FNH	FNH vs. HH
AP						
40	74.15 (54.18)	62.04 (20.15)	58.32 (47.92)	0.407	0.985	0.589
50	48.04 (35.43)	42.05 (14.65)	41.27 (36.32)	0.438	0.778	0.727
60	33.63 (23.01)	31.79 (12.21)	34.00 (24.50)	0.659	0.665	0.924
70	23.63 (15.87)	21.77 (7.81)	23.16 (17.35)	0.643	0.624	0.775
80	21.84 (7.10)	20.42 (5.83)	19.89 (10.86)	0.316	0.585	0.727
90	23.60 (4.95)	19.87 (8.73)	22.82 (7.54)	0.152	0.721	0.727
100	24.24 (6.80)	19.71 (12.44)	22.88 (5.92)	0.337	0.836	0.193
110	23.00 (7.59)	20.26 (14.06)	21.16 (4.60)	0.407	0.985	0.216
120	23.23 (8.71)	19.52 (12.42)	19.82 (3.55)	0.525	0.778	0.172
130	23.45 (9.56)	19.64 (12.36)	18.73 (2.92)	0.553	0.679	0.266
140	23.67 (10.21)	19.44 (13.13)	17.92 (2.42)	0.511	0.638	0.357
PP						
40	125.30 (73.50)	52.41 (30.98)	54.04 (18.74)	<0.001*	0.778	0.001*
50	81.20 (46.81)	35.60 (16.82)	39.27 (11.48)	<0.001*	0.440	0.001*
60	54.92 (31.65)	25.12 (13.28)	31.96 (6.28)	<0.001*	0.463	0.001*
70	39.25 (21.45)	17.61 (8.43)	21.41 (4.70)	<0.001*	0.283	0.002*
80	32.81 (13.96)	18.22 (5.73)	18.30 (3.85)	<0.001*	0.865	0.001*
90	28.89 (8.62)	21.07 (10.46)	20.15 (5.14)	<0.001*	0.463	0.001*
100	27.20 (5.05)	21.02 (10.67)	19.20 (6.34)	0.011*	0.275	0.001*
110	24.88 (6.76)	20.76 (11.82)	17.73 (6.82)	0.054	0.251	0.003*
120	24.86 (8.45)	20.67 (13.16)	16.73 (7.17)	0.200	0.236	0.006*
130	24.72 (10.42)	20.86 (14.19)	15.98 (7.39)	0.258	0.236	0.010*
140	24.31 (11.75)	20.01 (15.08)	15.44 (7.55)	0.337	0.221	0.010*

Data are expressed as median (interquartile range). *p<0.05. AP: arterial phase; FNH, focal nodular hyperplasia; HCC, hepatocellular carcinoma; HH, hepatic hemangioma; PP, portal venous phase.

Table 4. Quantitative assessment of HCC, HH and FNH with CT spectral imaging

	HH, *n*=17	HCC, *n*=31	FNH, *n*=7	*p*		
				HCC vs. HH	HCC vs. FNH	FNH vs. HH
IDM in the AP (water mg/mL)	0.75 (0.70)	2.04 (1.51)	3.34 (2.56)	<0.001*	0.080	0.006*
IDM in the PP (water mg/mL)	1.73 (1.00)	2.56 (1.17)	3.53 (1.09)	0.002*	0.052	0.017*
WDM in the AP (iodine mg/mL)	1,037.77 (11.12)	1,038.99 (12.22)	1,046.02 (20.98)	0.872	0.087	0.105
WDM in the PP (iodine mg/mL)	1,038.22 (16.80)	1,035.67 (12.53)	1,047.36 (22.31)	0.643	0.010*	0.039*
ICR	0.45 (0.18)	0.81 (0.26)	0.95 (0.10)	<0.001*	0.118	<0.001*
IUR in the AP	1.22 (0.61)	2.70 (1.75)	6.94 (6.39)	<0.001*	0.001*	<0.001*
IUR in the PP	0.57 (0.30)	0.93 (0.32)	1.18 (0.29)	0.002*	0.009*	0.002*
NIC in the AP	0.06 (0.06)	0.17 (0.13)	0.29 (0.08)	<0.001*	0.002*	0.002*
Slope in the AP	1.01 (0.98)	2.78 (2.06)	4.54 (2.45)	<0.001*	0.008*	<0.001*
Slope in the PP	2.34 (1.36)	3.48 (1.58)	4.80 (1.32)	0.007*	0.004*	0.001*

Data are expressed as median (interquartile range). *p<0.05. AP: arterial phase; FNH, focal nodular hyperplasia; HCC, hepatocellular carcinoma; HH, hepatic hemangioma; PP, portal venous phase.

Table 5. Qualitative CT assessment of lesions

Feature	HH, *n*=17	HCC, *n*=31	FNH, *n*=7	*p*		
				HCC vs. HH	HCC vs. FNH	FNH vs. HH
Necrosis or cyst	2 (11.8)	7 (22.6)	0 (0)	0.460	0.309	1
Central scars	2 (11.8)	0 (0)	4 (57.1)	0.121	0.001*	0.174
Presence of feeding vessels	0 (0)	15 (48.4)	6 (85.7)	<0.001*	0.104	<0.001*
Pseudocapsule	0 (0)	8 (25.8)	3 (42.9)	0.038	0.390	0.017*
Attenuation of enhancing area in AP						
Similar to aorta	7 (41.2)	0 (0)	0 (0)	<0.001*	–	0.065
Less than aorta, greater than adjacent liver parenchyma	10 (58.8)	31 (100)	7 (100)	<0.001*	–	0.065
Enhancement pattern in AP						
Globular or nodular	13 (76.5)	0 (0)	0(0)	<0.001*	–	<0.001*
Diffuse homogeneous	4 (23.5)	10 (32.3)	5 (71.4)	0.741	0.089	0.061
Diffuse heterogeneous	0 (0)	21 (67.7)	2 (28.6)	<0.001*	0.089	0.076
Enhancement change between AP and PP						
Expansion	14 (82.4)	0 (0)	4 (57.1)	<0.001*	0.001*	0.307
Washout	0 (0)	22 (71)	0 (0)	<0.001*	0.001*	–
None	3 (17.6)	9 (29)	4 (42.9)	0.497	0.203	0.134

Data represent number of lesions. Numbers in parentheses are percentages. The p-values were calculated using Fisher's exact test. *p<0.05; –, unable to calculate p-value using Fisher's exact test. FNH, focal nodular hyperplasia; HCC, hepatocellular carcinoma; HH, hepatic hemangioma.

PP, which was in line with the characteristics of "washout" feature of typical HCC during PP. While the value of IUR of FNH >1 during PP conformed to persistent enhancement characteristics of most FNH during PP. On the other hand, the value of IUR <1 in PP for HH, was contrary to the typically persistent enhancement feature. This could be due to the measurement of IDM in PP, including the part of HH without iodine filling during AP or PP. The ROI encompassed as much of the lesions as possible in order to measure the heterogeneity of lesion, and this caused the IUR in PP (IDM in PP of the lesion divided by the IDM in the PP of the liver) to be >1.

The present study did have some limitations. First, this was a retrospective study, with all the biases inherent to that study design. Second, this was a preliminary study with a small number of patients and needs to be verified by additional studies performed with a larger number of patients. Third, the HCCs in the present study were not classified by histopathological grade, because the numbers of patients in grades I and IV were too small. Fourth, because only one reader examined the images, intra- or inter-observer variability data were lacking. Fifth, and most importantly, there was a lack of correlation with conventional MDCT morphologic findings and typical features. Finally, quantitative analysis is time-consuming, and many of the described parameters could not be quantitated on picture archiving and communication system (PACS) and would need a dedicated AW workstation. Additional studies are necessary to address these issues.

Conclusions

In conclusion, spectral CT provides a set of monochromatic images, iodine-based MD images, and the quantitative parameters based on iodine concentration analysis that may help to increase the accuracy of the differentiation of HCC, HH, and FNH.

Acknowledgments

The authors are grateful to Dr. Jianying Li at GE Healthcare in revising the manuscript.

Funding

This work was supported by the National Natural Science Foundation of China (Grant number 81401406) and the Innovative Research Team of High-Level Local Universities in Shanghai.

Conflict of interest

The authors have no conflict of interests related to this publication.

Author contributions

Carried out the studies, participated in collecting data and drafted the manuscript (WL), carried out the studies and participated in collecting data (RL, XZ), participated in collecting data (YY, JZ), performed the statistical analysis and participated in its design (XL, WC), participated in acquisition and analysis of data (KC), participated in interpretation of data (FY). Manuscript writing and final approval of manuscript (all authors).

Data sharing statement

No additional data are available.

References

[1] Ferlay J, Soerjomataram I, Dikshit R, Eser S, Mathers C, Rebelo M, *et al*. Cancer incidence and mortality worldwide: sources, methods and major patterns in GLOBOCAN 2012. Int J Cancer 2015;136(5):E359–386. doi:10.1002/ijc.29210.
[2] Tapper EB, Parikh ND. Mortality due to cirrhosis and liver cancer in the United States, 1999-2016: observational study. BMJ 2018;362:k2817. doi:10.1136/bmj.k2817.
[3] Toro A, Mahfouz AE, Ardiri A, Malaguarnera M, Malaguarnera G, Loria F, *et al*. What is changing in indications and treatment of hepatic hemangiomas. A review. Ann Hepatol 2014;13(4):327–339.
[4] Marrero JA, Ahn J, Rajender Reddy K, Americal College of Gastroenterology. ACG clinical guideline: the diagnosis and management of focal liver lesions. Am J Gastroenterol 2014;109(9):1328–1347; quiz 1348. doi:10.1038/ajg.2014.213.
[5] Bioulac-Sage P, Laumonier H, Laurent C, Blanc JF, Balabaud C. Benign and malignant vascular tumors of the liver in adults. Semin Liver Dis 2008;28(3):302–314. doi:10.1055/s-0028-1085098.
[6] Demirjian A, Peng P, Geschwind JF, Cosgrove D, Schutz J, Kamel IR, *et al*. Infiltrating hepatocellular carcinoma: seeing the tree through the forest. J Gastrointest Surg 2011;15(11):2089–2097. doi:10.1007/s11605-011-1614-7.
[7] Llovet JM, Burroughs A, Bruix J. Hepatocellular carcinoma. Lancet 2003;362(9399):1907–1917. doi:10.1016/S0140-6736(03)14964-1.
[8] Trevisani F, Frigerio M, Santi V, Grignaschi A, Bernardi M. Hepatocellular carcinoma in non-cirrhotic liver: a reappraisal. Dig Liver Dis 2010;42(5):341–347. doi:10.1016/j.dld.2009.09.002.
[9] Leslie DF, Johnson CD, Johnson CM, Ilstrup DM, Harmsen WS. Distinction between cavernous hemangiomas of the liver and hepatic metastases on CT: value of contrast enhancement patterns. AJR Am J Roentgenol 1995;164(3):625–629. doi:10.2214/ajr.164.3.7863883.
[10] Lee JH, Lee JM, Kim SJ, Baek JH, Yun SH, Kim KW, *et al*. Enhancement patterns of hepatocellular carcinomas on multiphasicmultidetector row CT: comparison with pathological differentiation. Br J Radiol 2012;85(1017):e573–583. doi:10.1259/bjr/86767895.
[11] Quinn SF, Benjamin GG. Hepatic cavernous hemangiomas: simple diagnostic sign with dynamic bolus CT. Radiology 1992;182(2):545–548. doi:10.1148/radiology.182.2.1732978.
[12] Ito K, Mitchell DG, Outwater EK, Szklaruk J, Sadek AG. Hepatic lesions: discrimination of nonsolid, benign lesions from solid, malignant lesions with heavily T2-weighted fast spin-echo MR imaging. Radiology 1997;204(3):729–737. doi:10.1148/radiology.204.3.9280251.
[13] Farraher SW, Jara H, Chang KJ, Ozonoff A, Soto JA. Differentiation of hepatocellular carcinoma and hepatic metastasis from cysts and hemangiomas with calculated T2 relaxation times and the T1/T2 relaxation times ratio. J Magn Reson Imaging 2006;24(6):1333–1341. doi:10.1002/jmri.20758.
[14] Chan YL, Lee SF, Yu SC, Lai P, Ching AS. Hepatic malignant tumour versus cavernous haemangioma: differentiation on multiple breath-hold turbo spin-echo MRI sequences with different T2-weighting and T2-relaxation time measurements on a single slice multi-echo sequence. Clin Radiol 2002;57(4):250–257. doi:10.1053/crad.2001.0763.
[15] Cieszanowski A, Szeszkowski W, Golebiowski M, Bielecki DK, Grodzicki M, Pruszynski B. Discrimination of benign from malignant hepatic lesions based on their T2-relaxation times calculated from moderately T2-weighted turbo SE sequence. Eur Radiol 2002;12(9):2273–2279. doi:10.1007/s00330-002-1366-6.
[16] Santoro L, Grazioli L, Filippone A, Grassedonio E, Belli G, Colagrande S. Resovist enhanced MR imaging of the liver: does quantitative assessment help in focal lesion classification and characterization? J Magn Reson Imaging 2009;30(5):1012–1020. doi:10.1002/jmri.21937.
[17] Soyer P, Corno L, Boudiaf M, Aout M, Sirol M, Placé V, *et al*. Differentiation between cavernous hemangiomas and untreated malignant neoplasms of the liver with free-breathing diffusion-weighted MR imaging: comparison with T2-weighted fast spin-echo MR imaging. Eur J Radiol 2011;80(2):316–324. doi:10.1016/j.ejrad.2010.08.011.
[18] Turner MA, Fulcher AS. The cystic duct: normal anatomy and disease processes. Radiographics 2001;21(1):3–22; questionnaire 288-94. doi:10.1148/radiographics.21.1.g01ja093.
[19] Ruppert-Kohlmayr AJ, Uggowitzer MM, Kugler C, Zebedin D, Schaffler G, Ruppert GS. Focal nodular hyperplasia and hepatocellular adenoma of the liver: differentiation with multiphasic helical CT. AJR Am J Roentgenol 2001;176(6):1493–1498. doi:10.2214/ajr.176.6.1761493.
[20] van den Esschert JW, van Gulik TM, Phoa SS. Imaging modalities for focal nodular hyperplasia and hepatocellular adenoma. Dig Surg 2010;27(1):46–55. doi:10.1159/000268407.
[21] Sun M, Wang S, Song Q, Wang Z, Wang H, Ning D, *et al*. Utility of R2* obtained from T2*-weighted imaging in differentiating hepatocellular carcinomas from cavernous hemangiomas of the liver. PLoS One 2014;9(3):e91751. doi:10.1371/journal.pone.0091751.

[22] Jang HJ, Kim TK, Burns PN, Wilson SR. Enhancement patterns of hepatocellular carcinoma at contrast-enhanced US: comparison with histologic differentiation. Radiology 2007;244(3):898–906. doi:10.1148/radiol.2443061520.
[23] Okuda K. Hepatocellular carcinoma: recent progress. Hepatology 1992;15(5):948–963. doi:10.1002/hep.1840150532.
[24] Forner A, Vilana R, Ayuso C, Bianchi L, Solé M, Ayuso JR, *et al*. Diagnosis of hepatic nodules 20 mm or smaller in cirrhosis: prospective validation of the noninvasive diagnostic criteria for hepatocellular carcinoma. Hepatology 2008;47(1):97–104. doi:10.1002/hep.21966.
[25] Yoshikawa J, Matsui O, Takashima T, Ida M, Takanaka T, Kawamura I, *et al*. Fatty metamorphosis in hepatocellular carcinoma: radiologic features in 10 cases. AJR Am J Roentgenol 1988;151(4):717–720. doi:10.2214/ajr.151.4.717.
[26] Martín J, Sentís M, Zidan A, Donoso L, Puig J, Falcó J, *et al*. Fatty metamorphosis of hepatocellular carcinoma: detection with chemical shift gradient-echo MR imaging. Radiology 1995;195(1):125–130. doi:10.1148/radiology.195.1.7892452.
[27] Luo M, Zhang L, Jiang XH, Zhang WD. Intravoxel incoherent motion: application in differentiation of hepatocellular carcinoma and focal nodular hyperplasia. Diagn Interv Radiol 2017;23(4):263–271. doi:10.5152/dir.2017.16595.
[28] Leoni S, Piscaglia F, Golfieri R, Camaggi V, Vidili G, Pini P, *et al*. The impact of vascular and nonvascular findings on the noninvasive diagnosis of small hepatocellular carcinoma based on the EASL and AASLD criteria. Am J Gastroenterol 2010;105(3):599–609. doi:10.1038/ajg.2009.654.
[29] Moody AR, Wilson SR. Atypical hepatic hemangioma: a suggestive sonographic morphology. Radiology 1993;188(2):413–417. doi:10.1148/radiology.188.2.8327687.
[30] Vilgrain V, Boulos L, Vullierme MP, Denys A, Terris B, Menu Y. Imaging of atypical hemangiomas of the liver with pathologic correlation. Radiographics 2000;20(2):379–397. doi:10.1148/radiographics.20.2.g00mc01379.
[31] Kim T, Federle MP, Baron RL, Peterson MS, Kawamori Y. Discrimination of small hepatic hemangiomas from hypervascular malignant tumors smaller than 3 cm with three-phase helical CT. Radiology 2001;219(3):699–706. doi:10.1148/radiology.219.3.r01jn45699.
[32] Hanafusa K, Ohashi I, Himeno Y, Suzuki S, Shibuya H. Hepatic hemangioma: findings with two-phase CT. Radiology 1995;196(2):465–469. doi:10.1148/radiology.196.2.7617862.
[33] Hussain SM, Terkivatan T, Zondervan PE, Lanjouw E, de Rave S, Ijzermans JN, *et al*. Focal nodular hyperplasia: findings at state-of-the-art MR imaging, US, CT, and pathologic analysis. Radiographics 2004;24(1):3–17. discussion 18-9doi:10.1148/rg.241035050.
[34] Li J, Wang J, Lei L, Yuan G, He S. The diagnostic performance of gadoxetic acid disodium-enhanced magnetic resonance imaging and contrast-enhanced multi-detector computed tomography in detecting hepatocellular carcinoma: a meta-analysis of eight prospective studies. Eur Radiol 2019;29(12):6519–6528. doi:10.1007/s00330-019-06294-6.
[35] Hanna RF, Miloushev VZ, Tang A, Finklestone LA, Brejt SZ, Sandhu RS, *et al*. Comparative 13-year meta-analysis of the sensitivity and positive predictive value of ultrasound, CT, and MRI for detecting hepatocellular carcinoma. Abdom Radiol (NY) 2016;41(1):71–90. doi:10.1007/s00261-015-0592-8.
[36] Yang CB, Zhang S, Jia YJ, Yu Y, Duan HF, Zhang XR, *et al*. Dual energy spectral CT imaging for the evaluation of small hepatocellular carcinoma microvascular invasion. Eur J Radiol 2017;95:222–227. doi:10.1016/j.ejrad.2017.08.022.
[37] Pfeiffer D, Parakh A, Patino M, Kambadakone A, Rummeny EJ, Sahani DV. Iodine material density images in dual-energy CT: quantification of contrast uptake and washout in HCC. Abdom Radiol (NY) 2018;43(12):3317–3323. doi:10.1007/s00261-018-1636-7.
[38] Lv P, Lin XZ, Chen K, Gao J. Spectral CT in patients with small HCC: investigation of image quality and diagnostic accuracy. Eur Radiol 2012;22(10):2117–2124. doi:10.1007/s00330-012-2485-3.
[39] Altenbernd J, Heusner TA, Ringelstein A, Ladd SC, Forsting M, Antoch G. Dual-energy-CT of hypervascular liver lesions in patients with HCC: investigation of image quality and sensitivity. Eur Radiol 2011;21(4):738–743. doi:10.1007/s00330-010-1964-7.
[40] Marin D, Nelson RC, Samei E, Paulson EK, Ho LM, Boll DT, *et al*. Hypervascular liver tumors: low tube voltage, high tube current multidetector CT during late hepatic arterial phase for detection—initial clinical experience. Radiology 2009;251(3):771–779. doi:10.1148/radiol.2513081330.
[41] Große Hokamp N, Höink AJ, Doerner J, Jordan DW, Pahn G, Persigehl T, *et al*. Assessment of arterially hyper-enhancing liver lesions using virtual monoenergetic images from spectral detector CT: phantom and patient experience. Abdom Radiol (NY) 2018;43(8):2066–2074. doi:10.1007/s00261-017-1411-1.
[42] Shuman WP, Green DE, Busey JM, Mitsumori LM, Choi E, Koprowicz KM, *et al*. Dual-energy liver CT: effect of monochromatic imaging on lesion detection, conspicuity, and contrast-to-noise ratio of hypervascular lesions on late arterial phase. AJR Am J Roentgenol 2014;203(3):601–606. doi:10.2214/AJR.13.11337.
[43] Lv P, Lin XZ, Li J, Li W, Chen K. Differentiation of small hepatic hemangioma from small hepatocellular carcinoma: recently introduced spectral CT method. Radiology 2011;259(3):720–729. doi:10.1148/radiol.11101425.
[44] Laroia ST, Bhadoria AS, Venigalla Y, Chibber GK, Bihari C, Rastogi A, *et al*. Role of dual energy spectral computed tomography in characterization of hepatocellular carcinoma: Initial experience from a tertiary liver care institute. Eur J Radiol Open 2016;3:162–171. doi:10.1016/j.ejro.2016.05.007.
[45] Yu Y, Lin X, Chen K, Chai W, Hu S, Tang R, *et al*. Hepatocellular carcinoma and focal nodular hyperplasia of the liver: differentiation with CT spectral imaging. Eur Radiol 2013;23(6):1660–1668. doi:10.1007/s00330-012-2747-0.
[46] Yu Y, He N, Sun K, Lin X, Yan F, Chen K. Differentiating hepatocellular carcinoma from angiomyolipoma of the liver with CT spectral imaging: a preliminary study. Clin Radiol 2013;68(9):e491–497. doi:10.1016/j.crad.2013.03.027.
[47] Zhou L, Rui JA, Zhou WX, Wang SB, Chen SG, Qu Q. Edmondson-Steiner grade: a crucial predictor of recurrence and survival in hepatocellular carcinoma without microvascular invasio. Pathol Res Pract 2017;213(7):824–830. doi:10.1016/j.prp.2017.03.002.
[48] Wang Q, Shi G, Qi X, Fan X, Wang L. Quantitative analysis of the dual-energy CT virtual spectral curve for focal liver lesions characterization. Eur J Radiol 2014;83(10):1759–1764. doi:10.1016/j.ejrad.2014.07.009.